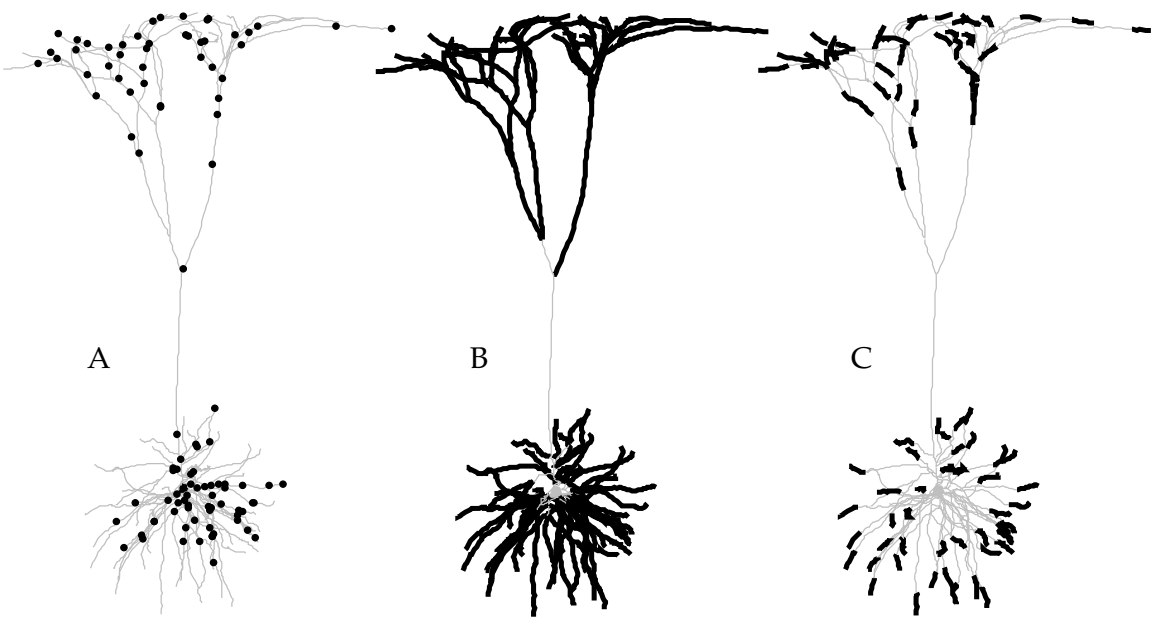


Figure 3: Voltage-dependent membrane mechanisms were spatially distributed in up to three different ways. A. When NMDA channels were present, they were restricted to activated spine heads. B,C. When spiking channel complexes were present, they were usually distributed in one of two spatial configurations: B. "Distal" configuration, in which channels were uniformly spread throughout the dendritic membrane except the main apical trunk and the proximal basal dendrites (shown in grey). Apical branches were labelled "distal" where their diameters fell below 2 mm (shown in black). C. In the "branch points" configuration, channels were confined to 40 $\mu$m segments at each distal branch point and branch tip (shown in black).

*hoc* fashion, a second, entirely different slow-spiking mechanism was implemented to act as a form of control. It was reasoned that if two functionally distinct slow-spiking mechanisms gave rise to very similar dendritic responses in a wide variety of tests, then the biophysical details of either should be of reduced importance—at least with respect to the questions being investigated here. The second slow-spiking mechanism was implemented according to the modified Hodgkin-Huxley formalism as before, with slowed kinetics to give a 10 ms spike width, and a modified voltage dependence to give a raised firing threshold from -50 mV to approximately -40 mV (fig. 2G; see $I_{slow-in}$ & $I_{slow-out}$ in Table 2). In numerous simulation experiments using one or the other or these very different slow-spiking mechanisms in the dendrites, no functionally significant differences were observed in relation to dendritic integration in the way studied here.

*Layout of Active Conductances*

As described above, the three mechanisms used in these simulations were 1) NMDA-type synapses, 2) fast spikes, and 3) slow spikes. These three voltage-dependent mechanisms, if present in a given run, were each distributed in one of three configurations in the dendritic arbor. NMDA-type synaptic channels, when present, were placed only on those spine heads that were to be activated during a given simulation run. The effective spatial distribution of NMDA synapses during a given run was therefore random and sparse (fig. 3A).

The fast and slow spiking mechanisms were inserted directly into the dendritic shaft membrane rather than on spine heads, and were spatially distributed in one of two global configurations. In the "distal" configuration, a spiking mechanism was uniformly distributed throughout the dendritic arbor, with the exception of the most proximal 60 $\mu$m length of each basal dendrite, and the main apical shaft to a distance of approximately 450 $\mu$m from the cell body where the branch diameters fell below 2 mm (fig. 3B). In the "branch point" configuration, the spiking mechanism was confined to the distal 40 $\mu$m segment of each distal apical branch, and to the distal 40 $\mu$m of each apical and basal dendritic tip (fig. 3C). Neither of these specific configurations was strongly motivated. The "distal" configuration essentially represents generic coverage of most of the dendritic tree; the proximal segments were avoided when in pilot simulations the presence of powerful spiking conductances in these dendrites resulted in anomalous voltage behavior at the cell body. The "branch point" configuration was motivated by the speculation, frequently raised in the experimental (Llinas & Nicholson 1971; Wong et al. 1979; Llinas & Sugimori 1980; Poolos & Kocsis 1990) and modeling (Shepherd et al. 1985; Shepherd & Brayton 1987; Rall & Segev 1987; Shepherd & Woolf 1989) literature that active dendritic conductances may be localized in discrete patches across the dendritic tree. One basis for this speculation is the observation of spikes of different heights ellicited in response to intradendritic current injection.

Many combinations of the three types of voltage-dependent mechanisms

| | $I_{\mathrm{Na}}$ | $I_{\mathrm{DR}}$ | $I_{\mathrm{Ca}}$ | $I_{\mathrm{KCa}}$ | $I_{\mathrm{slow-in}}$ | $I_{\mathrm{slow-out}}$ |
|---|---|---|---|---|---|---|
| $f_{open}$ | $m^2h$ | $m^2$ | $m^2$ | $m$ | $m^2h$ | $m^2$ |
| $V_{\frac{1}{2}}$ (mV) | -40,-45 | -40 | -35 | – | -25, -30 | -20 |
| $K$ | -3, 3 | -3 | -4 | – | -3, 3 | -3 |
| $\tau$ (ms) | 0.05, 0.5 | 2 | 2 | – | 0.6, 6.0 | 12 |
| $E_{rev}$ (mV) | 40 | -95 | 115 | -95 | 40 | -95 |
| Dendritic $\overline{g}$ ($S/cm^2$) | 0.1 | 0.05 | 0.001 | 0.008 | 0.05 | 0.02 |
| Somatic $\overline{g}$ ($S/cm^2$) | 0.4 | 0.2 | – | – | – | – |

Table 2: Modified Hodgkin-Huxley Parameters. Double entries (separated by commas) are for activation and inactivation particles. Peak dendritic conductances $\overline{g}$ were for conditions with single spiking complex in dendrites. When both spiking complexes were present, peak conductances were usually reduced. Rate and time constants for $I_{\mathrm{KCa}}$ were both voltage and calcium dependent, and were thus handled differently (see text).

dependence, respectively. The time constants $\tau_m$ and $\tau_h$ were assumed to be voltage independent. All parameters are summarized in Table 2.

*Two Slow-Spiking Mechanisms*

Two different mechanisms were used to generate slow dendritic spikes. The first was a calcium spiking mechanisms based on 1) an inward current through a high-threshold non-inactivating calcium channel, similar to an L channel, 2) an outward current through a calcium- and voltage-dependent potassium channel, and 3) calcium diffusion, buffering, and extrusion. The calcium channel was implemented using parameters as in Table 2. The potassium channel was taken from Moczydlowski and Latorre (1983), as included with the nmodl package within NEURON. Diffusion was one-dimensional and radial (D = 0.6 $\mu m^2$/ms), and discretized in four concentric compartments (as provided in NEURON). Longitudinal diffusion was ignored. Buffering kinetics within each diffusion shell $i$ were as follows:

$$\mathrm{Ca_i} + \mathrm{Buf_i} \underset{\mathrm{k_R}}{\overset{\mathrm{k_F}}{\rightleftharpoons}} \mathrm{BoundBuf_i},$$

with $k_F$ = 100/mM-ms, $k_R$ = 0.1/ms. Total buffer was $\sum_{i=0}^{4} = 30\mu M$. Calcium extrusion was modeled as simple exponential decay of calcium concentration in the outer shell, with a time constant of ~60 ms.

A spike generated by this mechanisms is shown in fig. 2E. The fast rising phase is driven by the activation of the voltage-dependent calcium channel; rapid increases in voltage and calcium concentration then activate the voltage and calcium-dependent potassium current, causing the membrane to be repolarized over 10-20 ms. Given the considerable uncertainty in the many parameter settings used in this channel complex, including those associated with calcium buffering, pumping, and diffusion, which were chosen in an *ad*

near the soma), and was on average approximately three times greater for apical vs. basal dendrites. In the experiments presented here, therefore, peak synaptic conductance was scaled to the input resistance measured locally at the spine head. This scaling procedure forced a rough but convenient correspondence between the size of a cluster of active synapses and the size of the local peak depolarization due to the clustered synaptic activity—independent of dendritic locus. While on its face this procedure implies that synapses on thick proximal trunks are much stronger than those on thin distal branchlets, a strong synapse may be viewed as consisting of a group of weaker synapses in close proximity, without loss of generality in any of the following results or discussions. In a typical high-NMDA test condition, the nominal peak NMDA conductance value $\overline{g}_{\mathrm{N}}$ ranged from 3.6 nS near the cell body to 0.2 nS on a distal apical tip, with an average value of 0.95 nS, as compared to peak AMPA conductance values one tenth as large, i.e. 0.36/0.02/0.095 nS. In zero-NMDA runs, peak AMPA conductance values ranged from 1.5 nS near the soma to 0.09 nS on a distal apical tip, with an average of 0.48 nS. For the AMPA channels, the peak conductance value $\overline{g}_{\mathrm{A}}$ is achieved during each synaptic event, independent of the local membrane voltage.

## Dendritic Spiking Mechanisms

The motivation to study the effects of dendritic spiking mechanisms comes primarily from intradendritic and other recording experiments in hippocampal pyramidal cells (Wong et al. 1979; Benardo *et al.* 1982; Mayakawa & Kato 1986; Andersen et al. 1987; Turner et al. 1989; Poolos & Kocsis 1990), and most recently intradendritic recordings in neocortical pyramids (Amitai *et al.* 1993). In both types of cells, intradendritic current injections were shown to give rise to complex superpositions of fast and slow dendritic spikes. In hippocampal pyramids, fast dendritic spikes were found to be mediated by sodium, based on their sensitivity to TTX (Wong et al. 1979; Benardo *et al.* 1982), while slow spikes were inferred to be calcium-mediated based on their elimination in zero-$Ca^{2+}$ solution (Poolos & Kocsis 1990). A recent optical recording study used $Ca^{2+}$- and $Na^{+}$-sensitive dyes simultaneously, confirming the participation and interaction of both ionic species in the generation of spikes in the dendrites of CA1 hippocampal pyramidal cells (Jaffe et al. 1992).

### *Fast Spiking Mechanism*

In the present simulations, a fast-spiking mechanism was used in the cell body and in some cases in the dendritic membrane. This mechanism consisted of a fast inward sodium current $I_{Na}$ and an outward current carried by a delayed rectifier $I_{DR}$ (fig. 2D). A modified Hodgkin-Huxley formalism (Bernander 1993) was used to compute the currents as a function of voltage and time (fig. 2D). Each "gating" term (e.g. m, h) obeyed first-order kinetics, with steady state values of the form $m_\infty = 1/[1 + e^{(V - V_{\frac{1}{2}})/K}]$, where $V_{\frac{1}{2}}$ and $K$ were the half-activation voltage and slope of the sigmoidal voltage

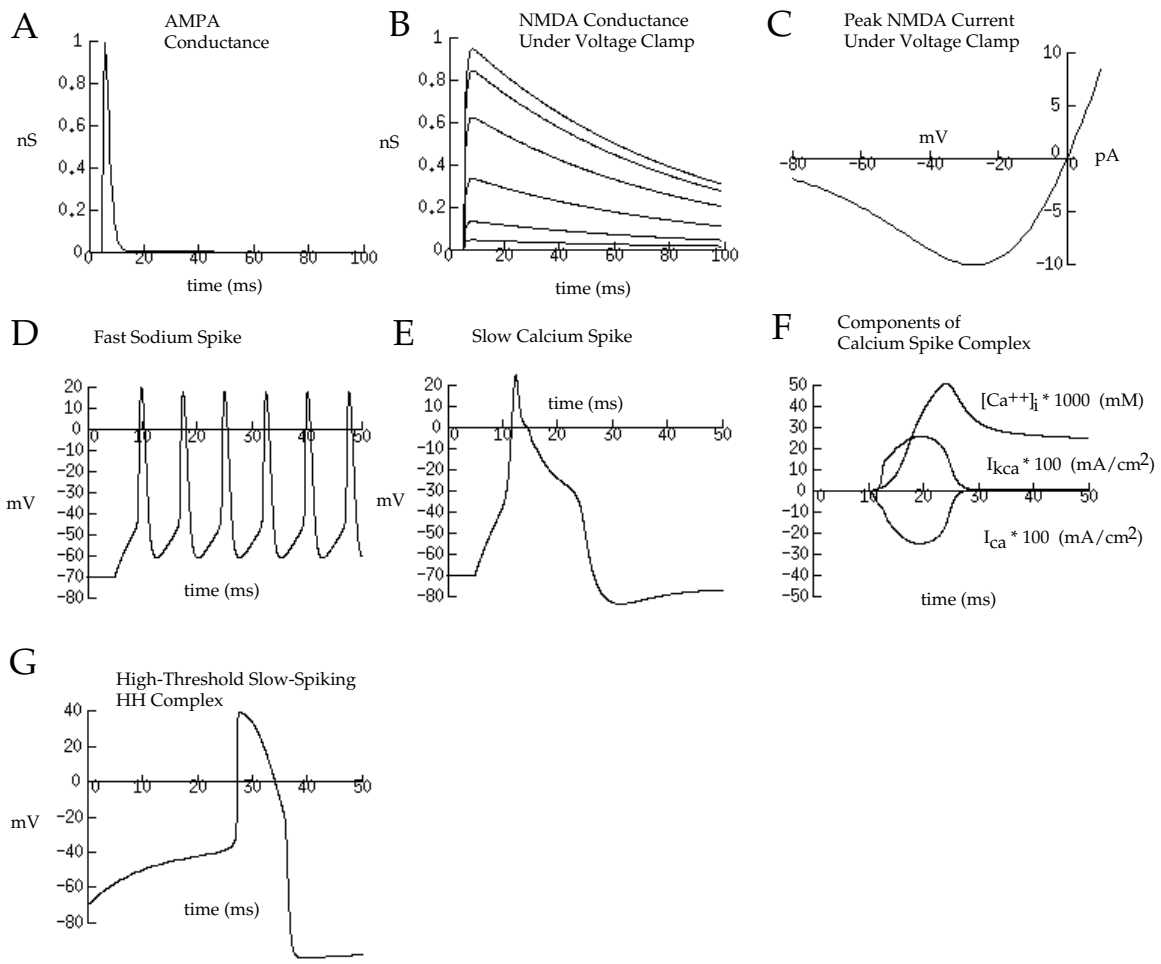


Figure 2: Waveforms describing channels used in simulations. A. Voltage-independent (AMPA) synapse is modeled as a fast-rising alpha function with $\tau = 1$ ms and $\overline{g}_{\mathrm{A}} = 1$ nS. B. NMDA-type synapse has a long-duration (compare to A) voltage-dependent conductance waveform, shown under simulated voltage-clamp for $\overline{g}_{\mathrm{N}} = 1$ nS. Lowest trace is at holding potential of -70 mV. Conductance waveform is repeated at 20 mV depolarizing increments. C. As a result of voltage-dependent conductance increases, NMDA channel also injects current in a voltage-dependent manner. As membrane is depolarized (under voltage clamp) from resting potential of -70 mV to -30 mV, peak injected current grows by a factor of 3. D. Fast-spiking conductance pair is minor variant of Hodgkin-Huxley. E. Slow-spiking complex contains a high-threshold, non-inactivating voltage-dependent calcium channel, a calcium and voltage-dependent potasium channel, and calcium buffering, diffusion, and extrusion. Resulting spike is 10-20 ms in width. F. Plotted are inward calcium current, internal calcium concentration, and outward potasium current (in a ball and stick model) during the generation of the spike in E. G. HH-type spike waveform with slowed kinetics and raised threshold, used as control for parameter sensitivity. Spiking channel parameters are shown in Table 2.

The voltage-independent AMPA conductance was modeled as an alpha function (fig. 2A):

$$G_{\mathrm{A}} = \overline{g}_{\mathrm{A}} \kappa t e^{-t/\tau}, \tag{0.1}$$

with $\overline{g}_{\mathrm{A}}$ the peak AMPA conductance, $\kappa = e/\tau$, and time to peak $\tau$ = 1 ms. The NMDA conductance depended exponentially on membrane voltage $V_m$ and on time, modeled as follows (Jahr & Stevens 1990a,b; Zador *et al.* 1990; fig. 2BC):

$$G_{\mathrm{N}} = \overline{g}_{\mathrm{N}} \frac{e^{-t/\tau_1} - e^{-t/\tau_2}}{1 + \eta[\mathrm{Mg}^{2+}]e^{-(\gamma V_m)}}, \tag{0.2}$$

with $\overline{g}_{\mathrm{N}}$ the nominal peak NMDA conductance, $\tau_1$ = 80 ms, $\tau_2$ = 0.66 ms, $\eta$ = 0.33/mM, $[\mathrm{Mg}^{2+}]$ = 1 mM, and $\gamma$ = 0.06/mV. The exponential voltage dependence appearing in the denominator represents the fact that the NMDA channel is blocked by magnesium ions at membrane voltages around (and more negative than) the resting potential, a block which is relieved at more depolarized potentials. The 80 ms time constant reflects both slow unbinding of glutamate from the NMDA-receptor and slow channel kinetics (Lester et al. 1990; Hestrin et al., 1990). The slow decay of the NMDA conductance leads to the possibility of summation of synaptic conductance across a train of spikes to a given synapse, however the maximum available NMDA conductance at each synapse was assumed to be $\overline{g}_{\mathrm{N}}$. This saturation condition corresponds to the assumption of many transmitter molecules released with each pre-synaptic event, but relatively few post-synaptic receptor sites. Non-saturating NMDA conductances were considered in (Mel 1992a).

In a given simulation run, every excitatory synapse contained the same fixed proportion of peak NMDA and AMPA conductance. The relative importance of NMDA vs. AMPA channels for normal synaptic transmission in neocortex has been partially assessed in selective pharmacological blocking studies. A dominant role for NMDA current was suggested in cat primary visual cortex, where visually-evoked responses in many cells were strongly attenuated (Fox *et al.* 1990) or eliminated (Miller *et al.* 1989) in the presence of the NMDA blocker APV. The exact proportion of NMDA to AMPA-type synaptic conductance is not, however, known with sufficient precision to tightly constrain our model. The proportions used in the present modeling experiments were thus set in one of two conditions designed to span the range of possibilities: 1) zero-NMDA, and 2) high-NMDA. In the high-NMDA condition, nominal peak NMDA conductance was set ten times larger than peak AMPA conductance, i.e. $\overline{g}_{\mathrm{N}} = 10\ \overline{g}_{\mathrm{A}}$. Note, however, that the voltage dependence of the NMDA channel is such that the *actual* NMDA conductance peak achieved during synaptic stimulation falls considerably short of the nominal peak value. For example, at a depolarized membrane potential of -30 mV (fig. 2C), the denominator of eqn. 0.2 is $\sim$3, such that the NMDA conductance actually achieved is only one third of the nominal peak conductance.

For the cell and parameters used in this study, the input resistance measured at a spine head varied by almost a factor of 17 depending on its dendritic location (roughly 2,200 M$\Omega$ on a distal apical dendrite vs. 133 M$\Omega$

| | |
|---|---|
| $R_m$ | $10,000\ \Omega\text{cm}^2$ |
| $C_m$ | $1.0\mu F/\text{cm}^2$ |
| $R_i$ | $200\ \Omega$cm |
| Input resistance at soma[1] | 24 M$\Omega$ |
| Time constant | 10 ms |
| Resting potential | -70 mV |
| Dendritic spines | $l = 1.0\ \mu$m, $d = 0.15\ \mu$m |
| Synaptic stimulation | 100 Hz with randomized interspike interval |
| Active synapses | 100, stimulated asynchronously |
| High-NMDA condition[2] | $\overline{g}_{\text{N}} = 3.6/0.2/0.95$ nS, $\overline{g}_{\text{A}} = 0.1\ \overline{g}_{\text{N}}$ |
| 0-NMDA condition[2] | $\overline{g}_{\text{A}} = 1.5/0.09/0.48$ nS |
| NMDA Parameters | $\eta = 0.33/\text{mM}$, $[\text{Mg}^{2+}] = 1$ mM, and $\gamma = 0.06/\text{mV}$ |
| Time constants | AMPA: $\tau = 1$ ms, NMDA: $\tau_1 = 80$ ms, $\tau_2 = 0.66$ ms |
| Synaptic reversal potential | 0 mV (both AMPA and NMDA) |
| Compartments | 473 plus 1 per activated dendritic spine |
| Compartment length | 40 $\mu$m |
| Integration time step | 0.1 ms |

Table 1: Simulation Parameters. [1]Input resistance, time constant, and resting potential for entirely passive cell. Somatic HH channels were essentially inactivated at rest (see Table 2), and thus had little effect on these values. [2]Peak conductances for NMDA ($\overline{g}_{\text{N}}$) and AMPA ($\overline{g}_{\text{A}}$) synapses were scaled to the local input resistance. Thus, conductance triples given for high-NMDA and 0-NMDA conditions were typical values for peak synaptic conductances near the soma, on a distal dendritic tip, and averaged over the arbor.

compartment. The axon was not modeled, as its fine diameter represented a negligible conductance load relative to the much thicker dendritic processes. Passive membrane parameters are given in Table 1.

## Modeling NMDA and Non-NMDA Synaptic Conductances

Excitatory synapses onto neocortical pyramidal cells make up around 85% of the 10,000 or more synaptic contacts (Beaulieu & Colonnier 1985). The major component of excitatory synaptic action onto these cells is thought to be mediated by glutamate. Two broad classes of glutamate-sensitive receptor subtypes have been characterized, associated with 1) a voltage-independent fast AMPA-type conductance, and 2) a voltage-dependent long-lasting NMDA-type conductance (Mayer & Westbrook 1987).

for a neurobiological model. First, direct monosynaptic connections between units with multiplicative input stages can implement a very general class of nonlinear associations (Feldman & Ballard 1982; Giles & Maxwell 1987; Durbin & Rumelhart 1989; Mel 1990; Mel & Koch 1990; Poggio & Girosi 1990; Koch & Poggio 1992). Second, the learning of such associations can be achieved with a simple Hebbian rule of a general type known to exist in the central nervous system (Bliss & Lømo 1973; Brown *et al.* 1988b; Sejnowski & Tesauro 1989). Third, numerous suggestions have been made over the past decade that voltage-dependent membrane mechanisms in dendritic trees could afford the multiplicative interactions among neighboring synapses needed for this type of model neuron (Feldman & Ballard 1982; Koch & Poggio 1987; Rall & Segev 1987; Shepherd & Brayton 1987; Brown *et al.* 1988b; Shepherd *et al.* 1989; Durbin & Rumelhart 1989; Mel 1990; Mel & Koch 1990; Poggio & Girosi 1990; Brown *et al.* 1991).

The theoretical appeal of the sigma-pi unit as a biological model thus motivated the main experimental paradigm used in this paper. Sigma-pi-like behavior in a real neuron might be evidenced by differential cell responses to patterns of synaptic input that differ in the degree of spatial clustering of the activated synapses. The present goal was to test whether biologically plausible distributions of voltage-dependent ionic conductances in a dendritic tree could render activation of synapses in clusters more effective than activation of the same number of synapses scattered diffusely across the dendritic tree.

# Methods

## Compartmental Modeling

A compartmental modeling program called NEURON was used to carry out the simulations reported in this work (Michael Hines, personal communication). Anatomical data from an HRP-filled reconstructed layer 5 pyramidal cell from cat visual cortex was provided by Rodney Douglas and Kevan Martin. More than 3,000 measurements of branch length and diameter were consolidated into 163 connected dendritic branch sections, consisting of 10 basal dendrites leaving the soma, culminating in 56 basal branch tips, and a main apical shaft terminating in an apical tuft with 31 apical branch tips (see fig. 3). The cell used here was mapped into approximately 500 isopotential "compartments", each representing at most $40\mu$m segment of dendritic length. Since the available anatomical data did not encode the locations and structural parameters of dendritic spines, a scheme proposed by Stratford et al. (1989) was used to increment the length and diameter of each dendritic branch in order that its area, input resistance, axial resistance, and effective electrotonic length mimicked those of a branch covered with spines at an assumed density of one spine per micron (see Larkman 1991; Douglas & Martin 1990). For each synapse that was to be explicitly activated during a simulation run, an additional compartment representing a cylindrical spine of length $1\mu$m and diameter $0.15\mu$m was attached to the main dendritic branch

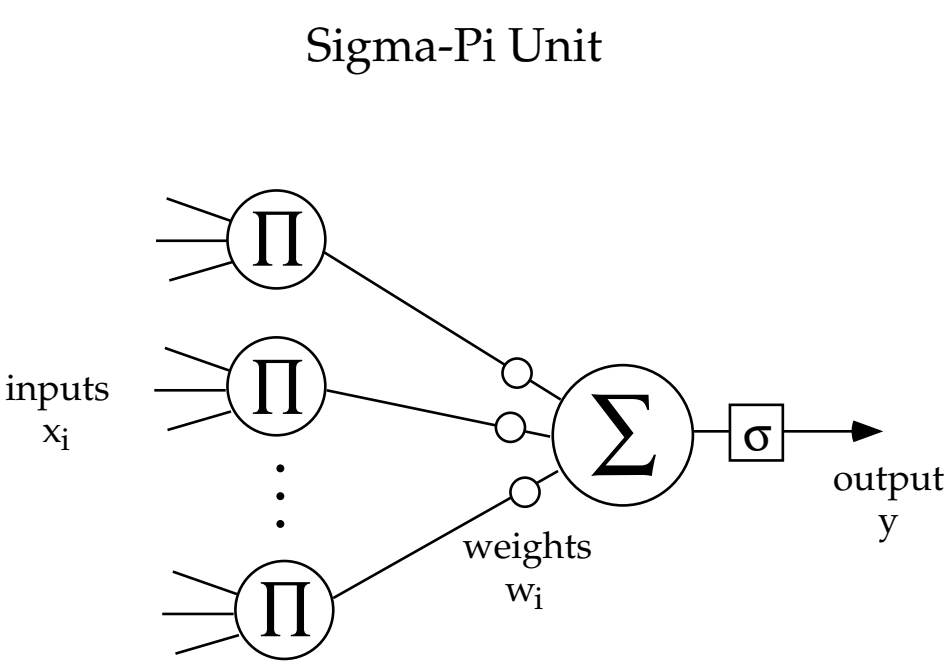


Figure 1: A sigma-pi unit is an abstract model neuron that sums contributions over independent multiplicative clusters of input synapses, $y = \sigma(\sum_i w_i \Pi x_{ik} \cdots x_{il})$, where $i$ indexes the cluster, and $\sigma$ is an optional sigmoidal nonlinearity applied to the sum of products. A single unit is thus a multi-layered network in and of itself, where each multiplicative cluster acts as a nonlinear "hidden unit".

"logic-spots" might be strategically incorporated into dendritic membrane as needed to implement arbitrary logical computations in the dendritic tree (Shepherd & Brayton 1987; Shepherd et al. 1989; Zador et al. 1992). While all of these studies have been sources of valuable intuition as to the possibilities for information processing in a dendritic tree, none has addressed the more realistic case of tree-wide synaptic integration in excitable dendrites when tens to hundreds of synapses are coactivated in complex spatial patterns.

## A Motivating Hypothesis

The main goal of the current study, as for (Mel 1992a), was to explore the validity of a simple, essentially statistical hypothesis as to the input-output behavior of a dendritic tree containing excitatory voltage-dependent conductances, that depends little on the detailed geometry of the dendritic arbor, the precise strength or spatial distribution of active membrane conductances, their kinetics, or their voltage-dependencies.

Our initial hypothesis was derived from a simple abstract model neuron, called a *sigma-pi* neuron (Rumelhart et al. 1986; Mel 1990). A sigma-pi neuron computes its output as a weighted sum of contributions from a set of independent multiplicative clusters of synaptic inputs, in analogy with the weighted sum of multiplicative terms in a polynomial function (fig. 1).

Three factors have recommended this single-unit abstraction as the seed

# Introduction

Despite many decades of anatomical and physiological study, a basic understanding of the input-output behavior of the neocortical pyramidal cell is still lacking. What kind of "device" is a pyramidal cell, in the sense that one might ask of a transistor or a logic gate extracted from a computer circuit? How does it transform a complex pattern of synaptic input into an output firing rate? In short, what does a single neocortical pyramidal cell compute?

Experimental techniques do not yet exist that allow this question to be studied directly. As dendritic branch diameters are commonly 1$\mu$m or less, intradendritic recordings in neocortical pyramids have been extremely rare; those recordings that do exist have been taken only from main apical trunks (Amitai et al. 1993). Even as optical recording techniques grow increasingly sophisticated, allowing transmembrane voltage and/or intracellular ion concentrations to be imaged over large regions of a dendritic tree (Grinvald et al. 1981; Tank et al. 1988; Regehr et al. 1989; Guthrie et al. 1991; Müller & Connor 1991; Jaffe et al. 1992), it is not yet possible to selectively stimulate large numbers of afferent fibers that make synaptic contacts onto a dendritic tree at specific locations. Such precise stimulus control would be needed to directly probe mechanisms of spatio-temporal integration of synaptic input under "natural" stimulus conditions. Given the enormous technical hurdles that remain before direct experimental verification of hypotheses becomes possible, biophysically-realistic compartmental modeling techniques remain the most powerful and flexible methodological approach to this question.

In early modeling work, dendritic trees were often conceptualized as electrically passive branched cable-like structures (see Jack et al. 1975; Rall 1977; Segev 1992; Mel 1993). Both classical and more recent work on passive dendritic information processing has most often concerned 1) passive spatio-temporal integration of synaptic inputs (Rall, 1964; Poggio & Torre 1978; Koch et al. 1982; Borg-Graham & Grzywacs 1992), 2) dendritic subunit structure (Koch et al. 1982; Miller & Bloomfield 1983; Woolf et al. 1991), or 3) the effects of synaptic background activity on passive cable structure (Holmes & Woody 1989; Bernander et al. 1991; see also Laurent & Burrows 1989).

Other studies have considered possible roles of *active* membrane in dendrites or on spine heads in dendritic information processing (Rall & Shepherd 1968; Miller et al. 1985; Perkel & Perkel 1985; Shepherd et al. 1985; Rall & Segev 1987; Wilson 1992). For example, Rall and Segev (1987) modeled dendritic branches on which subsets of spines contained excitable membrane. Several different types of interactions were observed depending on the spatial distribution of active vs. passive spine heads. It was suggested that the observed sensitivity to the distribution of active spine heads and input conditions could allow for a rich repertoire of logical operations among neighboring synapses. Indeed, others have demonstrated that appropriate localization of patches of voltage-dependent membrane could implement logical operations such as AND, OR, and XOR operations, with the suggestion that these

# Summary and Conclusions

1. Compartmental modeling experiments were carried out in an anatomically characterized neocortical pyramidal cell to study the integrative behavior of a complex dendritic tree containing active membrane mechanisms. Building on a hypothesis presented in (Mel 1992a), this work provides further support for a novel principle of dendritic information processing, that could underlie a capacity for nonlinear pattern discrimination and/or sensory-processing within the dendritic trees of individual nerve cells.

2. It was previously demonstrated that when excitatory synaptic input to a pyramidal cell is dominated by voltage-dependent NMDA-type channels, the cell responds more strongly when synaptic drive is concentrated within several dendritic regions than when it is delivered diffusely across the dendritic arbor (Mel 1992a). This effect, called dendritic "cluster sensitivity", persisted under wide ranging parameter variations, and directly implicated the spatial *ordering* of afferent synaptic connections onto the dendritic tree as an important determinant of neuronal response selectivity.

3. In this work, the sensitivity of neocortical dendrites to spatially clustered synaptic drive has been further studied with fast sodium and slow calcium spiking mechanisms present in the dendritic membrane. Several spatial distributions of the dendritic spiking mechanisms were tested, with and without NMDA synapses. Results of numerous simulations reveal that dendritic cluster sensitivity is a highly robust phenomenon in dendrites containing a sufficiency of excitatory membrane mechanisms, and is only weakly dependent on their detailed spatial distribution, peak conductances, or kinetics. Factors that either work against or make irrelevant the dendritic cluster sensitivity effect include 1) very high-resistance spine necks, 2) very large synaptic conductances, 3) very high baseline levels of synaptic activity, or 4) large fluctuations in level of synaptic activity on short time scales.

4. The functional significance of dendritic cluster-sensitivity has been previously discussed in the context of associative learning and memory (Mel 1992ab). Here it is demonstrated that the dendritic tree of a cluster-sensitive neuron implements an approximative spatial *correlation*, or sum of products operation, such as that which could underlie nonlinear disparity tuning in binocular visual neurons.

# Synaptic Integration in an Excitable Dendritic Tree

**Bartlett W. Mel**
*Computation and Neural Systems Program*
*Division of Biology, 216-76*
*California Institute of Technology*
*Pasadena, California 91125*
*mel@caltech.edu*

Running Head: Synaptic Integration in Excitable Dendrites
Telephone: (818)356-3643 (w), (213)913-1817 (h)
Fax: (818)796-8876